A ghost particle-based coupling approach for combined finite-discrete element method

***Hu Chen[1], †Y.X. Zhang[1] and Mengyan Zang[2]**

[1]School of Engineering and Information Technology, The University of New South Wales, ADFA, Canberra, ACT 2600, Australia
[2]School of Mechanical and Automotive Engineering, South China University of Technology, Guangzhou, China

*Presenting author: hu.chen@student.adfa.edu.au
†Corresponding author: y.zhang@adfa.edu.au

Abstract

Combined finite-discrete element method takes the advantages of both the finite element (FE) method and the discrete element (DE) method, but a coupling approach is required for effective combination of the two methods. In this paper, a coupling approach is proposed by using ghost particles. The entire domain is decomposed into a FE region and a DE region which are connected by an interface, and ghost particles are constructed inside the boundary of FEs by interpolation and used to connect the boundary of DEs. This interface connection method effectively couples FEs with DEs. A numerical example is computed to demonstrate the effectiveness of the proposed approach.

Keywords: Ghost particle, Coupling approach, Combined finite-discrete element method, Multiscale modelling.

Introduction

The conventional finite element (FE) method has some limitations in numerical modelling of brittle fracture problems since it is based on the continuum mechanics, and special treatments have to be employed, e.g., remeshing strategies [Mediavilla et al. (2006); Belytschko and Black (1999)] or extended finite element method [Belytschko et al. (2001); Moės and Belytschko (2002)]. In contrast, the discrete element (DE) method is able to capture the discontinuous nature of materials, but it is not as computational efficient as the FE method. Combined finite-discrete element method, which combines the two methods, has been developed so as to use the advantages while avoiding the drawbacks of the two numerical methods [Munjiza (2004)].

Essentially, the combination of the two methods can be achieved by the interaction of either contact or coupling. The contact interaction is more suitable for contact occurring between different pieces of an object when fragmentations form [Munjiza et al. (1995)] and between two or more different media [Onate and Rojek (2004); Chen et al. (2015)]. The coupling interaction is more applicable for the connection between different subdomains of an entire domain, which is decomposed for efficient computation via the so-called multiscale modeling. The coupling approaches used along with the combined finite-discrete element method are generally classified into overlapping coupling [Wellmann and Wriggers (2012); Li et al. (2015); Jebahi et al. (2013); Tu et al. (2014)] and interface coupling [Christian et al. (2014); Lei and Zang

(2010)]. For the overlapping coupling compatibility condition is required to be satisfied in a bridging domain [Xiao and Belytschko (2004)], where the total energy is a linear mixing of energies from both FEs and DEs, while only a simple compatibility condition at the interface is required to be satisfied in the interface coupling.

In this paper, a ghost particle-based approach is proposed to couple the continua with discrete elements for the combined finite-discrete element method. The computational domain is decomposed into a FE region and a DE region, which are distinguished by an interface. The two regions are connected by the interface interaction between the boundary DEs and ghost particles which are constructed at the boundary FEs. This approach is conceived from the extension of atomistic-continuum coupling [Kohlhoff et al. (1991); Shilkrot et al. (2002)], in which ghost atoms are used to coincide with the FE nodes in the transition region (harsh mesh requirement), and the number of coincidence layers is dependent on the cut-off radius of atomistic potential. For the present approach, however, only one layer of ghost particles is required as the interaction of DEs only occurs between adjacent particles. Furthermore, to overcome the difficulties of remeshing, the strictly coincident compatibility condition is relaxed by introducing the ghost particles, whose position is determined from the interpolation of nodal coordinates of FEs.

To apply this coupling approach to model fracture problems, an important and essential step is to validate its effectiveness prior to the occurrence of fractures. This paper is therefore confined to the development and validation of this new coupling approach, without exploration and investigation into brittle fractures. The governing equations and DE model will be briefly introduced in next section. Afterwards, the development of the proposed coupling approach is presented in detail, followed by the numerical validation. Finally, conclusions are drawn.

General formulations

The governing equations for FEs and DEs are briefly described first, followed by the introduction of a DE connective model, which is used to discretize the area of interest.

Governing equations

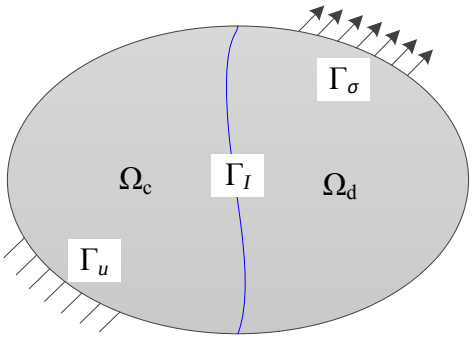

Figure 1. Domain decomposition into a continuum region and a discrete region

A computational domain, subject to prescribed displacement at the Dirichlet boundary Γ_u and prescribed tractions at the Neumann boundary Γ_σ, is divided into a continuum subdomain Ω_c and a discrete subdomain Ω_d as shown in Figure 1. The interface between these two subdomains is defined as $\Gamma_I = \partial\Omega_c \cap \partial\Omega_d$.

For the continuum subdomain, the FEs are used for spatial discretization and the governing equation of the FE method is given as

$$\mathbf{M}\ddot{\mathbf{U}} + \mathbf{K}\mathbf{U} = \mathbf{F} + \mathbf{F}^{\mathrm{cou}} \tag{1}$$

where **M** and **K** are mass and stiffness matrices, respectively; **U** is the displacement vector; **F** is the resultant force vector consisting of external tractions and/or damping force; $\mathbf{F}^{\mathrm{cou}}$ is the coupling force resulting from the interaction with the discrete subdomain.

The discrete subdomain is discretized by DEs and the equations of motion for each DE particle are expressed as follows

$$\begin{cases} m\dot{\mathbf{v}} = \mathbf{f} + \mathbf{f}^{\mathrm{cou}} \\ I\dot{\boldsymbol{\omega}} = \mathbf{t} + \mathbf{r} \times \mathbf{f}^{\mathrm{cou}} \end{cases} \tag{2}$$

where m is the mass of the particle; **v** is the centroid velocity of the particle in global coordinate frame; **f** is the resultant force applied to the particle due to (a) external traction, (b) body force, (c) internal force when the DE connective model is used and (d) damping force (linearly proportional to the velocity) to dissipate kinetic energy for computational purpose; $\mathbf{f}^{\mathrm{cou}}$ is the coupling force exerted on the particle resulting from the interaction with the continuum subdomain; I is the moment of inertia of the particle; **ω** is the angular velocity of the particle in the local coordinate frame which is embedded into the centroid of the particle; **t** is the resultant moment applied to the particle due to the aforementioned forces **f**; **r** is the moment arm of the coupling force $\mathbf{f}^{\mathrm{cou}}$.

Discrete element model

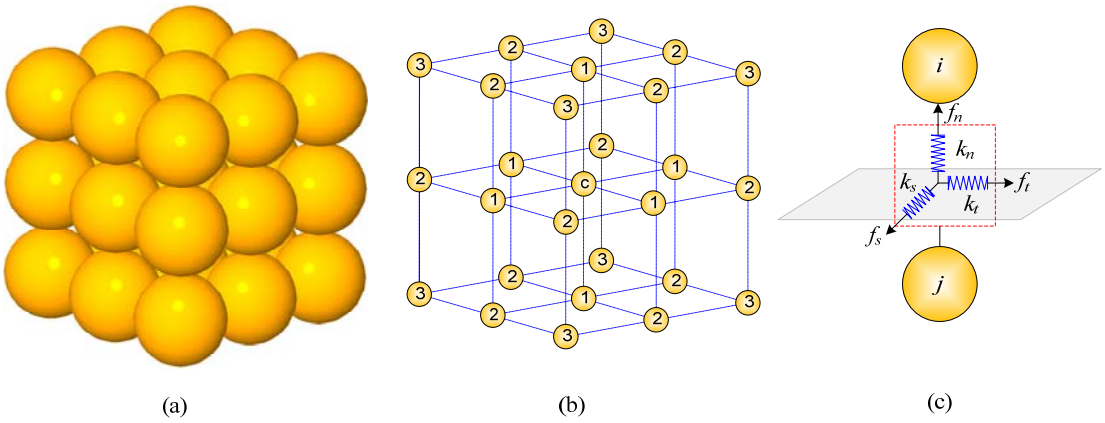

Figure 2. The discrete element connective model. (a) Cubic arrangement of the 27 spherical particles. (b) Linkage relation. (c) Virtual springs connect adjacent particles.

The DE connective model as shown in Figure 2 is employed. This model is in a cubic arrangement (Figure 2a), which can produce a neat surface desirable for domain decomposition. Each particle in this model is connected to its neighboring 26 particles, which are categorized into three groups according to their distances to the central one as depicted by different numbers in Figure 2b. The interaction force **f** between any two adjacent particles is calculated based on their relative displacement **d** and spring stiffness k (see Figure 2c) as follows

$$\mathbf{f} = k\mathbf{d} \tag{3}$$

where force $\mathbf{f} = (f_n, f_s, f_t)$,and $\mathbf{d} = (d_n, d_s, d_t)$.

Inside each pair as shown in Figure 2c, there are an orthogonal (k_n) and two tangential (k_s and k_t) linear springs invisibly connecting them. Their stiffness are determined based on the energy equivalence between the one stored in the springs and that in solid elasticity, as given by [Yu (2011)]

$$\begin{cases} k_n^1 = k_n^2 = \dfrac{2Er}{5(1-2\nu)} \\ k_s^1 = k_t^1 = k_s^2 = k_t^2 = \dfrac{2Er(1-4\nu)}{5(1-2\nu)(1+\nu)} \\ k_n^3 = k_s^3 = k_t^3 = 0 \end{cases} \tag{4}$$

where E, ν and r are the Young's modulus, Poisson's ratio and radius of the DE particles.

Coupling approach

The coupling force is explicitly expressed through the interaction between the boundary DE particles and the ghost particles, which are virtually constructed at the inside of boundary hexahedral elements. Next, the strategy of constructing ghost particles is illustrated first, followed by the determination of natural coordinates and the kinematic relations between DE boundary particles and ghost particles.

Construction of ghost particles

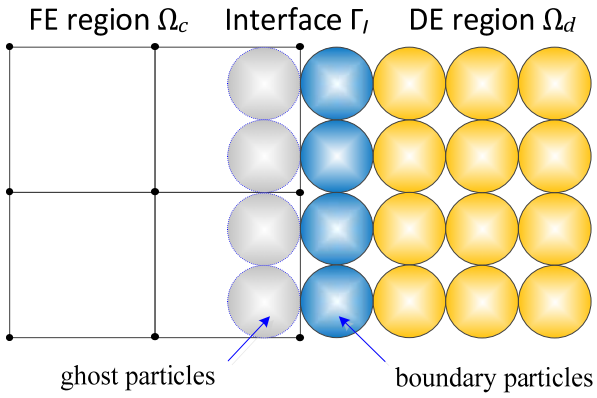

Figure 3. Schematic diagram of the coupling approach

A general rule to decompose domain is that the DE particles are used to spatially discretize the region of particular interest, such as the impact zone or area where fractures possibly occur, whereas the other region is discretized by FEs. Usually, the radius of DE particles is much smaller than the size of FEs to better characterize fracture patterns. The DE region should be large enough to cover the interest zone so as to avoid possible fractures occurring in the continuum region. Therefore, it is not necessary to generate a flexible but uncontrollable interface and a neat interface as shown in Figure 3 is then utilized for easy model preprocessing.

Ghost particles are constructed inside the FEs as shown in Figure 3, and they can be treated as a part of the DE model. Each DE particle only interacts with its adjacent particles; hence one layer of ghost particles is adequate to describe the coupling

interaction between boundary DE particles and ghost particles. The interaction mechanism between them is the same as that for a sole DE model as shown in Eqs. (3) and (4), and particularly, this interaction interconnects the FE model and the DE model. Note that these ghost particles and DE particles should have the same radius for the application of this interaction mechanism to link them together. Because only one layer of ghost particles is required and also the size of them is small, the ghost particles are merely constructed in the boundary FEs.

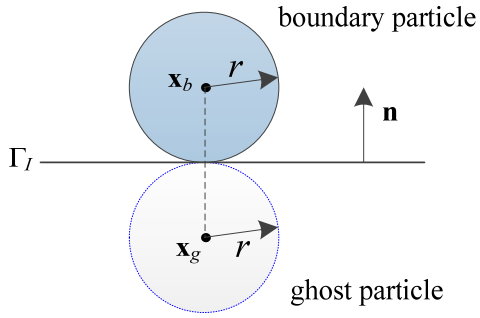

Figure 4. Position determination of the ghost particle

As a virtual part of the corresponding FE, each ghost particle has the same kinematic response as that of the FE when subject to loading or deformation. With this compatibility condition taken into account, a reasonable assumption is made that each ghost particle sticks to the same natural coordinate of the corresponding isoparametric FE. The natural coordinates will be determined next, but before doing so, the physical coordinates of ghost particles need to be acquired. As being symmetric to the boundary DE particles (as shown in Figure 4), the physical coordinates of ghost particles at initial configuration can be immediately determined by

$$\mathbf{x}_g = \mathbf{x}_b - 2r\mathbf{n} \tag{5}$$

where $\mathbf{x}_g$ and $\mathbf{x}_b$ are physical coordinates of boundary particles and ghost particles; $\mathbf{n}$ is the normal vector of interface.

Determination of natural coordinates

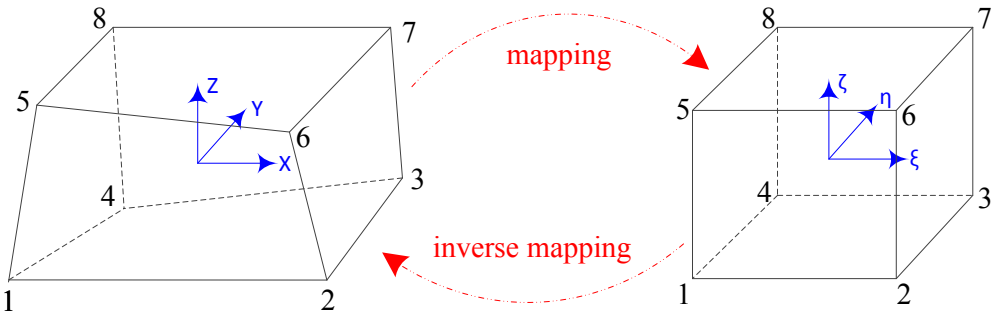

Figure 5. Mapping and inverse mapping between physical coordinates and natural coordinates

For any ghost particles, their physical coordinates can be obtained from Eq. (5), thus the purpose here is to determine corresponding unknown natural coordinates.

For a given point $\mathbf{x}$ located inside a hexahedron element, the physical coordinate (x, y, z) of that point can be expressed by the interpolation from nodal coordinates and their associated shape functions $N(\xi, \eta, \zeta)$ as follows

$$\mathbf{x} = \mathbf{x}(\xi, \eta, \zeta) = \sum_{I=1}^{8} N_I(\xi, \eta, \zeta)\mathbf{x}_I \tag{6}$$

The shape functions are specifically given

$$N_I = \frac{1}{8}(1 + \xi_I\xi)(1 + \eta_I\eta)(1 + \zeta_I\zeta) \tag{7}$$

where the natural coordinate for each node I is shown in Table 1.

Table 1. Natural coordinate for each node, $\boldsymbol{\xi}_I = (\xi_I, \eta_I, \zeta_I)$

$\boldsymbol{\xi}_1 = (-1, -1, -1)$	$\boldsymbol{\xi}_2 = (+1, -1, -1)$
$\boldsymbol{\xi}_3 = (+1, +1, -1)$	$\boldsymbol{\xi}_4 = (-1, +1, -1)$
$\boldsymbol{\xi}_5 = (-1, -1, +1)$	$\boldsymbol{\xi}_6 = (+1, -1, +1)$
$\boldsymbol{\xi}_7 = (+1, +1, +1)$	$\boldsymbol{\xi}_8 = (-1, +1, +1)$

It is worth noting that Eq. (6) indicates the mapping from physical coordinates to natural coordinates (shown in Figure 5); however, its inverse mapping from natural coordinates to physical coordinates, i.e., $\boldsymbol{\xi} = \boldsymbol{\xi}(x, y, z)$, is generally impossible to be explicitly expressed [Belytschko et al. (2013)]. Note that here we use position vectors to denote specific coordinates, i.e., $\mathbf{x} = (x, y, z)$ and $\boldsymbol{\xi} = (\xi, \eta, \zeta)$. Therefore, to specifically determine natural coordinates, an alternative numerical approach [Qian et al. (1998)] based on Taylor series is employed.

The position vector of physical coordinates as seen in Eq. (6) is expanded around $\mathbf{x}_o = (x_o, y_o, z_o)$ with a linear approximation

$$\mathbf{x} \approx \mathbf{x}_o + \frac{\partial \mathbf{x}(\xi_o, \eta_o, \zeta_o)}{\partial \boldsymbol{\xi}}(\boldsymbol{\xi} - \boldsymbol{\xi}_o) \tag{8}$$

where Jacobian matrix $\mathbf{J} = \partial \mathbf{x}/\partial \boldsymbol{\xi}$ is specifically given by

$$\mathbf{J} = \begin{vmatrix} \frac{\partial x}{\partial \xi} & \frac{\partial x}{\partial \eta} & \frac{\partial x}{\partial \zeta} \\ \frac{\partial y}{\partial \xi} & \frac{\partial y}{\partial \eta} & \frac{\partial y}{\partial \zeta} \\ \frac{\partial z}{\partial \xi} & \frac{\partial z}{\partial \eta} & \frac{\partial z}{\partial \zeta} \end{vmatrix} \tag{9}$$

and $\boldsymbol{\xi}_\mathbf{o}$ is the corresponding natural coordinates of $\mathbf{x}_\mathbf{o}$, i.e., $\mathbf{x}_\mathbf{o} = \mathbf{x}(\xi_o, \eta_o, \zeta_o)$.

Rearranging Eqs. (8) and (9), an iterative form for natural coordinates is expressed as follows

$$\boldsymbol{\xi}_{k+1} \approx \boldsymbol{\xi}_k + \mathbf{J}_k^{-1}(\mathbf{x} - \mathbf{x}_k) \;\; (k = 0,1,2\cdots) \tag{10}$$

where $\mathbf{x}_k = \mathbf{x}(\xi_k, \eta_k, \zeta_k)$. The iteration is terminated when the $\mathcal{L}_2$ norm is less than a user-specified tolerance ε, i.e.,

$$\|\mathbf{x} - \mathbf{x}_k\|_2 < \varepsilon \tag{11}$$

As the natural coordinates only need to be determined once at the initial configuration when hexahedron elements are not deformed yet, this numerical iteration is very efficient to achieve its convergence.

Interaction between particles

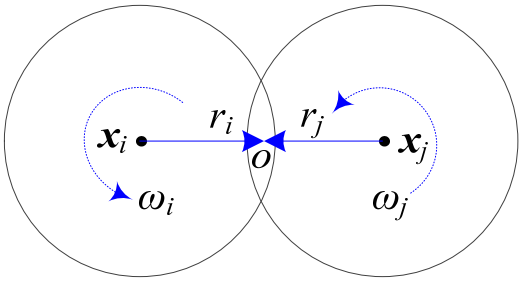

Figure 6. Kinematic relation of two adjacent particles

For any two adjacent particles (i and j) as shown in Figure 6, their interaction force can be calculated by Eq. (3). As the stiffness of springs keeps constant, the practical interest here is to determine their relative displacement. With the central difference method employed for temporal discretization, an incremental form is used to calculate the relative displacement at t_{n+1}

$$\mathbf{d}_{n+1} = \mathbf{d}_n + \Delta\mathbf{d}_{n+1} \tag{12}$$

where the incremental relative displacement $\Delta\mathbf{d}_{n+1}$ is determined by relative velocity as follows

$$\Delta\mathbf{d}_{n+1} = \dot{\mathbf{x}}^{ij}_{n+1/2}\Delta t_{n+1} \tag{13}$$

At any time, the relative velocity is evaluated at the middle point o of the line connecting two particles' centroids, as expressed by

$$\dot{\mathbf{x}}^{ij} = \dot{\mathbf{x}}^j_o - \dot{\mathbf{x}}^i_o \tag{14}$$

in which

$$\begin{cases} \dot{\mathbf{x}}^i_o = \dot{\mathbf{x}}^i + \boldsymbol{\omega}^i \times \mathbf{r}^i \\ \dot{\mathbf{x}}^j_o = \dot{\mathbf{x}}^j + \boldsymbol{\omega}^j \times \mathbf{r}^j \end{cases} \tag{15}$$

where $\dot{\mathbf{x}}^i$ and $\dot{\mathbf{x}}^j$ are velocities of the particle i and j, respectively.

If one of the particles in the pair is a ghost one, its rotational velocity is not taken into account and the translational velocity is interpolated from the nodal velocities of the corresponding FE as follows

$$\dot{\mathbf{x}} = \sum_{I=1}^{8} N_I(\xi, \eta, \zeta)\dot{\mathbf{x}}_I \tag{16}$$

where the natural coordinate $\boldsymbol{\xi} = (\xi, \eta, \zeta)$ is determined using the method mentioned before.

It is worth noting that the interaction force exerted on each ghost particle is distributed into all nodes of the corresponding FE with the use of shape functions as given by Eq (17).

$$\mathbf{f}_I = -N_I(\xi, \eta, \zeta)\mathbf{f} \tag{17}$$

Numerical validation

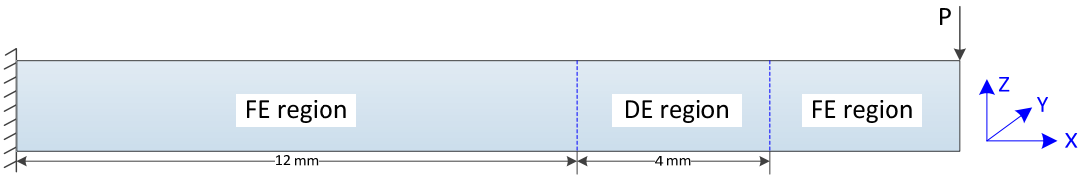

Figure 7. Diagram of the cantilever beam and the particles distribution in the coupled finite-discrete element model.

To validate the proposed numerical method, the coupling approach is implemented in an in-house code named as CDFP [Lei and Zang (2010)]. A cantilever beam with one end fixed and the other subject to constant loading ($P = 0.4$ N) as shown in Figure 7 is modeled, and the computed deflection at the free end of the beam is compared to the analytical result.

The dimensions of this beam are: length $L = 20$ mm, width $W = 4$ mm and height $H = 2$ mm. The elastic material properties are: mass density $\rho = 0.001$ g/mm^3, Young's modulus $E = 1000$ MPa and Poisson's ratio $\nu = 0.23$. The coupled finite element model with the FE and DE regions as allocated in Figure 7 is generated by using different spatial discretization techniques. The mesh size for both the FE model and the coupled model is 0.5 mm and the particle radius for both the DE model and the coupled model is 0.125 mm. To acquire a static solution from the explicit central difference time integration, an appropriate damping is imposed to the nodal and particle velocities.

The deflection at the free end computed from the coupled model is 0.388 mm, which is very close to the analytical solution 0.4 mm. To further demonstrate the effectiveness of the proposed coupling model, the displacement distribution of the beam along the loading direction obtained from the FE model, the DE model and the coupled model are compared in Figure 8, where a good agreement can be observed.

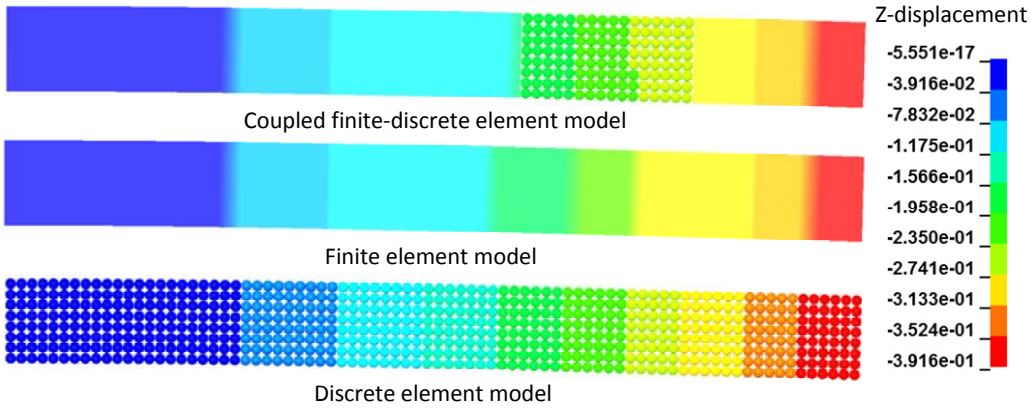

Figure 8. The comparison of displacement distributions along loading direction.

Conclusions

In this paper a new approach to couple continua with DEs is proposed by using ghost particles. The ghost particles are constructed at the boundary FEs to connect DEs and this connection is achieved through the same interaction mechanism as the DE method. To keep ghost particles constantly sticking to the same natural coordinates of the corresponding FEs, an iterative strategy for inverse mapping from physical coordinates to natural coordinates is employed. The proposed numerical approach is used to model a cantilever beam and the agreement of the computed deflection at the free end with the analytical result validates the numerical method.

Acknowledgement

The PhD scholarship awarded to Hu Chen from UNSW Canberra and the China Scholarship Council is gratefully acknowledged.

References

Mediavilla, J., Peerlings, R. H. J., and Geers, M. G. D. (2006) A robust and consistent remeshing-transfer operator for ductile fracture simulations, *Computers & Structures* **84**, 604-623.

Belytschko, T. and Black, T. (1999) Elastic crack growth in finite elements with minimal remeshing, *International Journal for Numerical Methods in Engineering* **45**, 601-620.

Belytschko, T., Moës, N., Usui, S., and Parimi, C. (2001) Arbitrary discontinuities in finite elements, *International Journal for Numerical Methods in Engineering* **50**, 993-1013.

Moës, N. and Belytschko, T. (2002) Extended finite element method for cohesive crack growth, *Engineering Fracture Mechanics* **69**, 813-833.

Munjiza, A. (2004) *The combined finite-discrete element method*, John Wiley & Sons, West Sussex.

Munjiza, A., Owen, D., and Bicanic, N. (1995) A combined finite-discrete element method in transient dynamics of fracturing solids, *Engineering Computations* **12**, 145-174.

Onate, E. and Rojek, J. (2004) Combination of discrete element and finite element methods for dynamic analysis of geomechanics problems, *Computer Methods in Applied Mechanics and Engineering* **193**, 3087-3128.

Chen, H., Zhang, Y. X., Zang, M., and Hazell, P. J. (2015) An accurate and robust contact detection algorithm for particle-solid interaction in combined finite-discrete element analysis, *International Journal for Numerical Methods in Engineering*, doi: 10.1002/nme.4913.

Wellmann, C. and Wriggers, P. (2012) A two-scale model of granular materials, *Computer Methods in Applied Mechanics and Engineering* **205–208**, 46-58.

Li, M., Yu, H., Wang, J., Xia, X., and Chen, J. (2015) A multiscale coupling approach between discrete element method and finite difference method for dynamic analysis, *International Journal for Numerical Methods in Engineering* **102**, 1-21.

Jebahi, M., Charles, J. L., Dau, F., Illoul, L., and Iordanoff, I. (2013) 3D coupling approach between discrete and continuum models for dynamic simulations (DEM-CNEM), *Computer Methods in Applied Mechanics and Engineering* **255**, 196-209.

Tu, F., Ling, D., Bu, L., and Yang, Q. (2014) Generalized bridging domain method for coupling finite elements with discrete elements, *Computer Methods in Applied Mechanics and Engineering* **276**, 509-533.

Christian, M., Françoise, L. P., and Ludovic, A. (2015) A least-squares coupling method between a finite element code and a discrete element code, *International Journal for Numerical Methods in Engineering* **101**, 731-743.

Lei, Z. and Zang, M. (2010) An approach to combining 3D discrete and finite element methods based on penalty function method, *Computational Mechanics* **46**, 609-619.

Xiao, S. P. and Belytschko, T. (2004) A bridging domain method for coupling continua with molecular dynamics, *Computer Methods in Applied Mechanics and Engineering* **193**, 1645-1669.

Kohlhoff, S., Gumbsch, P., and Fischmeister, H. F. (1991) Crack propagation in b.c.c. crystals studied with a combined finite-element and atomistic model, *Philosophical Magazine A* **64**, 851-878.

Shilkrot, L. E., Miller, R. E., and Curtin, W. A. (2002) Coupled Atomistic and Discrete Dislocation Plasticity, *Physical Review Letters* **89**, 025501.

Yu, J., Analysis and application of the algorithm by combining discrete and finite element method in plane. 2011, South China University of Technology: Guangzhou, China.

Belytschko, T., Liu, W. K., and Moran, B. (2013) *Nonlinear finite elements for continua and structures*.

Qian, X., Ren, Q., and Zhao, Y. (1998) An algorithm for inverse isoparametric mapping in FEM, *Chinese Journal of Computational Mechanics* **15**, 437-441.